AMERICAN ACADEMY OF OPHTHALMOLOGY®

Cellular Determinants of Visual Outcomes in Eyes with Epiretinal Membrane: Insights from Adaptive Optics OCT

Masaharu Ishikura, MD, PhD, Yuki Muraoka, MD, PhD, Naomi Nishigori, MD, Takahiro Kogo, MD, Yuki Akiyama, MD, Shogo Numa, MD, PhD, Masayuki Hata, MD, PhD, Kenji Ishihara, MD, PhD, Sotaro Ooto, MD, PhD, Akitaka Tsujikawa, MD, PhD

Objective: In this study, we aimed to evaluate cellular alterations in the foveal neuroglia of eyes with idiopathic epiretinal membrane (ERM) and examine their correlation with visual function. We also aimed to identify prognostic markers for visual outcomes postvitrectomy.

Design: A prospective longitudinal study.

Subjects: The study comprised 84 subjects, including 50 eyes diagnosed with idiopathic ERM and 34 healthy eyes serving as controls.

Methods: The foveal neuroglial changes in eyes with idiopathic ERM were determined using adaptive optics OCT (AO-OCT) by comparing them with healthy eyes. For patients with ERM, the ERM and inner limiting membrane were removed during vitrectomy in all eyes.

Main Outcome Measures: Foveal microstructures on AO-OCT images, best-corrected visual acuity (BCVA) and M-CHARTS scores, evaluated preoperatively and at 1, 3, and 6 months postoperatively, and associations between foveal neuroglial changes and these parameters.

Results: Adaptive optics OCT revealed discernible differences in the foveal cones of the eyes with ERM and their healthy counterparts. The thickness of the ellipsoid zone (EZ) band was augmented in eyes with ERM. The alignment of the Müller cells was more vertical and the density of the foveal cone cell nuclei was higher in eyes with ERM than in healthy eyes. Within the AO-OCT parameters, the higher cone nuclei count correlated with worse M-CHARTS scores, both preoperatively and 6 months postoperatively ($P = 0.004$, 0.010, respectively). Greater EZ thickness was significantly associated with poorer 6-month postoperative BCVA ($P = 0.005$).

Conclusions: Adaptive optics OCT can be used to precisely identify cellular alterations in eyes with ERM that are closely related to visual function impairments. These cellular insights enhance our understanding of ERM pathology and offer promising prognostic indicators of visual outcome after vitrectomy. *Ophthalmology Science 2024;4:100536 © 2024 by the American Academy of Ophthalmology. This is an open access article under the CC BY-NC-ND license (http://creativecommons.org/licenses/by-nc-nd/4.0/).*

Supplemental material available at www.ophthalmologyscience.org.

Epiretinal membrane (ERM) is highly prevalent in middle-aged and older adults.[1,2] Epiretinal membrane is characterized by a contractile membrane on the retinal surface that interacts with the retinal tissue in a complex manner.[3,4] This interaction can distort the neuroglia in multiple dimensions,[5,6] which can diminish visual acuity and induce metamorphopsia,[7] often necessitating vitrectomy. However, the degree of visual function improvement achieved postoperatively can vary, and predicting the postoperative outcomes remains a challenge in clinical practice.[8]

Spectral-domain (SD)OCT has previously identified features such as ectopic inner foveal layers,[9] and the central bouquet abnormalities including the cotton ball sign[10] in eyes with ERM.[11] Thus, it has an instrumental role in revealing the structural changes in eyes with ERM. These findings demonstrate the effect of ERM on the inner and outer retinal layers; however, a definitive link to visual function has not been established. Consequently, researchers have continued the pursuit of reliable prognostic markers in this field.

Recent advances in adaptive optics (AO) have improved the ability to visualize fine details of the retinal microstructures.[12–14] Adaptive optics OCT has enabled the visualization of individual photoreceptor nuclei and Müller cells in the healthy state[15] and in eyes afflicted by ERM.[16] These advancements have elucidated the influence of ERM on Müller cells and the subsequent effect on photoreceptor integrity; however, the association between these cellular changes and visual function remains unclear.

Therefore, in this study, we aimed to evaluate the retinal changes induced by ERM using AO-OCT to address this

https://doi.org/10.1016/j.xops.2024.100536
ISSN 2666-9145/24

gap in the literature. We investigated the neuroglial changes associated with reduced visual acuity and metamorphopsia in patients with ERM to determine the associations between neuroglial alterations and visual impairment and identify markers for predicting the postoperative visual outcomes.

Methods

Patients

This prospective, longitudinal study was conducted in strict accordance with the tenets of the Declaration of Helsinki. This study was approved by the Institutional Review Board and Ethics Committee of the Kyoto University Graduate School of Medicine (Kyoto, Japan). Written informed consent was obtained from the patients and healthy volunteers before commencing any study-related procedure or evaluation.

Patients diagnosed with idiopathic ERM at the Kyoto University Hospital between March 2021 and July 2023 were included in this study. This study period included diagnosis, surgery, and a 6-month postoperative observation. In addition, age-matched healthy volunteers with no history or evidence of systemic or macular diseases were also assessed. The diagnosis of idiopathic ERM was made based on the presence of fibrocellular tissue at the vitreoretinal interface on SD-OCT (Spectralis HRA + OCT; Heidelberg Engineering) images. The axial and lateral resolutions were 7 μm and 14 μm, respectively.

Eyes with secondary ERM, attributable to conditions such as ocular inflammation, retinal tears, or vascular occlusions, as well as those with tractional and degenerative lamellar holes, significant cataracts affecting vision, and any other factors potentially responsible for visual impairment other than idiopathic ERM, were excluded from this study. In addition, eyes that met specific ocular conditions such as glaucoma, intraocular pressure $\geq$21 mmHg, high myopia (exceeding -6 diopters), pronounced astigmatism (surpassing ± 3 diopters), or keratoconus, and eyes with low-quality Adaptive optics OCT images owing to involuntary eye movements or media opacification were excluded from this study. Adaptive optics OCT and SD-OCT imaging were conducted preoperatively and at 1, 3, and 6 months postoperatively to assess changes in retinal structure.

Surgical Procedure

All patients diagnosed with ERM underwent vitrectomy performed by an experienced surgeon (Y.M.) with over a decade of expertise in vitreoretinal surgeries. The surgeries were conducted using a 27-gauge four-port transconjunctival vitrectomy approach, with 1 of the ports specifically dedicated to a chandelier light source. This surgical setup was selected to improve intraoperative visualization, facilitating a thorough examination for potential peripheral retinal breaks that may not have been detected preoperatively. Importantly, our study protocol mandated the exclusion of any cases with retinal breaks identified either before or during the surgical procedure. Patients who had not previously undergone cataract surgery underwent phacoemulsification with intraocular lens implantation. We ensured the thorough removal of the macular ERM. The inner limiting membrane (ILM) of each patient was stained with Brilliant Blue G dye to facilitate clear visualization, covering an area >4 disc diameters centered on the macula. Removal was achieved through a meticulous pinch-and-peel technique, ensuring no ILM was left within the peeled area upon completion.

AO-OCT Imaging Protocol

An imaging device (CANON Inc) that can simultaneously capture AO-OCT and scanning laser ophthalmoscopy images was used. Axial and lateral resolutions of 3.4 μm and 3.0 μm, respectively, were achieved by correcting aberrations within the AO system. The AO-OCT device was focused to capture the foveal area spanning 2.5° (728 μm). These images were acquired at a rate of 45 frames/s over a 23-s duration for each retinal section and were subsequently combined using an integrated software. Adaptive optics scanning laser ophthalmoscopy imaging was used for retinal tracking during the capture process to ensure consistency in the imaging locations preoperatively and postoperatively.

Evaluation of the AO-OCT Images

Adaptive optics OCT was utilized to achieve a detailed visualization of individual cone cell nuclei within the outer nuclear layer. In addition, Müller cell bodies, appearing as hyporeflective, elongated structures within the retinal tissue, were identified. These structures were observed originating from the ILM and extending toward the external limiting membrane. The qualitative assessment of the regions containing Müller cells was performed by 2 independent readers (M.I. and Y.M.) who identified and described their appearance in the images.

Structural differences between conventional SD-OCT and AO-OCT were qualitatively examined. Qualitative and quantitative methods were performed using AO-OCT to identify the cellular configurations of the retinal neuroglia present in the fovea of healthy eyes and eyes with ERM. A comparative analysis of the preoperative and postoperative conditions of eyes affected by ERM was subsequently conducted.

The thickness of the entire retina and ellipsoid zone (EZ) (Fig S1) were derived using a method described previously.[17] The midpoint between the maximum and minimum reflectivity was calculated to determine the boundaries of the EZ band. Thereafter, the EZ thickness was determined using the full-width half-maximum method.

To quantify cone nuclei, we utilized the "Find Maxima" function in ImageJ, adopting a method similar to that previously reported by Kadomoto et al.[15] This function automatically identifies and measures hyperreflective dots, local maxima in the images, significantly brighter than their immediate surroundings. This process facilitates the objective quantification of cone cell nuclei within the outer nuclear layer by counting these hyperreflective dots, providing a standardized approach to

assessing retinal structure. Measurements along the horizontal plane were adjusted by correcting the axial length-related magnification owing to the potential variations in eye size using the modified Littmann formula (Bennett procedure),[18] taking into account the axial length of the eye.[17,18] Reflective structures suggestive of cone cell nuclei were evaluated within a distance of 400 μm centered on the foveola.

Statistical Analysis

All statistical analyses were performed using the JMP 16 software (SAS Institute Inc). All values are presented as mean ± standard deviation. We defined best-corrected visual acuity (BCVA) as the decimal visual acuity converted into logarithm of the minimum angle of resolution. Decimal visual acuity was measured individually for each eye using the Landolt chart at a distance of 5 m. Refractive error and astigmatism were assessed preoperatively and at 1, 3, and 6 months postoperatively using an autorefractor (ARK-530K; NIDEK). Based on the objective measurements, subjective refraction tests were conducted, and decimal visual acuity was measured. Finally, for statistical analysis, the measurements were converted to logarithm of the minimum angle of resolution. Retinal parameters with normal distribution were compared between healthy volunteers and patients with ERM using a *t*-test. Comparisons of systemic factors between healthy participants and patients with ERM were performed using the chi-square test for sex differences. Comparisons between the characteristics and analysis of AO-OCT findings of healthy participants and patients with ERM were performed using a 2-sided test. $P < 0.05$ was considered statistically significant.

The dependent variables in our study included preoperative visual acuity measured in logarithm of the minimum angle of resolution and the M-CHARTS score. The independent variables included retinal thickness at the fovea, the postoperative Cotton ball sign derived from SD-OCT, and AO-OCT parameters, such as EZ thickness and the number of cone cell nuclei within a specified width of 400 μm. These parameters included a stage classification and the presence or absence of the central bouquet abnormality in the outer retina. We classified the cases using preoperative SD-OCT images based on the stage classification reported by Govetto et al:[9] stage 1 was marked by the presence of a foveal pit, stage 2 was identified by the absence of the foveal pit but without any ectopic inner foveal layers, stage 3 was defined by continuous ectopic inner foveal layers and a clear retinal layer structure, and stage 4 was characterized by disrupted retinal layers. The central bouquet abnormality was further categorized as follows: a score of 2 was assigned for foveolar detachment, 1 for the presence of the cotton ball sign, and 0 if neither condition was present. A similar analysis, comparing the preoperative retinal parameters with postoperative visual outcomes, was conducted to evaluate the effect of the preoperative retinal parameters on the postoperative visual function.

Multiple linear regression analyses were performed using the least squares method to analyze the relationship between the preoperative and postoperative retinal structural parameters and visual function. Continuous variables were standardized using means and standard deviations, and standardized beta coefficients were derived to compare the effect of each independent variable on the dependent variable. Owing to the ordinal nature of the stage classification, dummy coding was used for ordinal variables to generate variables, such as stage 2 to stage 1 and stage 3 to stage 2, to incorporate ordinality into the regression models. To rigorously ensure the absence of multicollinearity in multiple linear regression analyses, the variance inflation factor for each explanatory variable was calculated. All variance inflation factor values were confirmed to remain below the threshold of 5, indicating that multicollinearity was not a concern.

Results

Baseline Characteristics and OCT Findings

Table 1 presents the baseline characteristics of the healthy volunteers and patients with ERM. This study comprised 50 eyes from 40 patients (16 males and 24 females) with idiopathic ERM, alongside a control group of 34 eyes from 34 age-matched healthy volunteers (11 males and 23 females). Age and sex distribution were comparable between the groups ($P = 0.90$, 0.50, respectively). All participants were Japanese. In this study, retinal breaks were not observed during any of the vitrectomy procedures. Based on the preoperative images obtained using SD-OCT, 32% (16/50), 36% (18/50), and 32% (16/50) of the eyes were classified as stages 1, 2, and 3, respectively. The cotton ball sign and foveolar detachment were observed in 22% (11/50) and 14% (7/50) of patients, respectively.

Longitudinal Changes in Visual Function and Foveal Morphology

A significant improvement in the visual outcomes was observed following vitrectomy, wherein ERM and ILM were excised. Over a 6-month period, the BCVA improved from a mean of 0.06 (Snellen equivalent range: 20/66−20/13) preoperatively to −0.04 (Snellen equivalent range: 20/33−20/13) postoperatively, whereas the M-CHARTS scores decreased from 0.54 preoperatively to 0.38 postoperatively. These changes were accompanied by a notable reduction in the whole retinal thickness (Fig 2). Postoperatively at 6 months, according to the SD-OCT parameters, the cotton ball sign was reduced to 6 cases (6/50), and foveolar detachment improved in all cases.

In the study, a roundish or diffuse highly reflective region was consistently observed between the photoreceptor inner segment/outer segment junction line and cone outer segment tips line at the center of the fovea. Adaptive optics OCT facilitated the visualization of individual cone cell nuclei and Müller cells, which presented as hyporeflective structures from the vitreoretinal interface to the external limiting membrane that were unobservable on SD-OCT images (Fig

Table 1. Baseline Characteristics of Healthy Participants and Patients with Idiopathic ERM

	Healthy Participants	Patients with ERM	*P*-Value
Number (men/women)	34 (11/23)	40 (16/24)	(0.50)*
Number (eyes)	34	50	n.a.
Age (years)	67.7 ± 11.1	67.4 ± 7.9	0.90†
Spherical equivalent (diopter)	−1.5 ± 1.8	−1.1 ± 1.9	0.31†
Axial length (mm)	23.9 ± 1.5	24.1 ± 1.3	0.53†
Visual acuity in logMAR	−0.07 ± 0.07	0.06 ± 0.13	<0.001†
Snellen visual acuity (range)	20/20–20/13	20/66–20/13	n.a.
M-CHARTS score (degree)	not evaluated	0.54 ± 0.44	n.a.
Intraocular pressure (mmHg)	14.4 ± 2.6	14.3 ± 3.2	0.92†
SD-OCT findings			
Staging of ERM			
Stage 1	n.a.	16 (32.0%)	n.a.
Stage 2		18 (36.0%)	
Stage 3		16 (32.0%)	
Stage 4		0 (0.0%)	
Central bouquet abnormality			
Cotton ball sign, n (%)	n.a.	11 (22.0%)	n.a.
Foveolar detachment, n (%)		7 (14.0%)	
Vitelliform lesion, n (%)		0 (0.0%)	

The data are shown as mean ± standard deviation unless otherwise indicated.
ERM = epiretinal membrane; logMAR = logarithm of the minimum angle of resolution; n.a. = not applicable; SD-OCT = spectral domain OCT.
Staging of ERM is based on classification reported by Govetto A and associates (Ref.[9]).
*Comparisons of systemic factors between healthy participants and patients with ERM were performed using the chi-square test for sex differences.
†Comparisons of systemic factors between healthy participants and patients with CSC were performed using t test.

3). Adaptive optics OCT also demonstrated vertical and anterior traction on the Müller cells caused by ERM, which resulted in increased EZ thickness and reflectivity (Fig 4). A notable shift in Müller cell alignment from diagonal to vertical direction was noted in eyes with ERM (Fig 5). Vertical traction derived from horizontal contractile forces on the retinal surface affected the photoreceptor layer via Müller cells (Figs 4 and 6). Additionally, there was an increase in the density of the cone nuclei (Figs 2, 5 and 7). However, the Müller cells reverted to the diagonal orientation after vitrectomy (Fig 3). The cone nuclei density decreased significantly from the baseline to 6

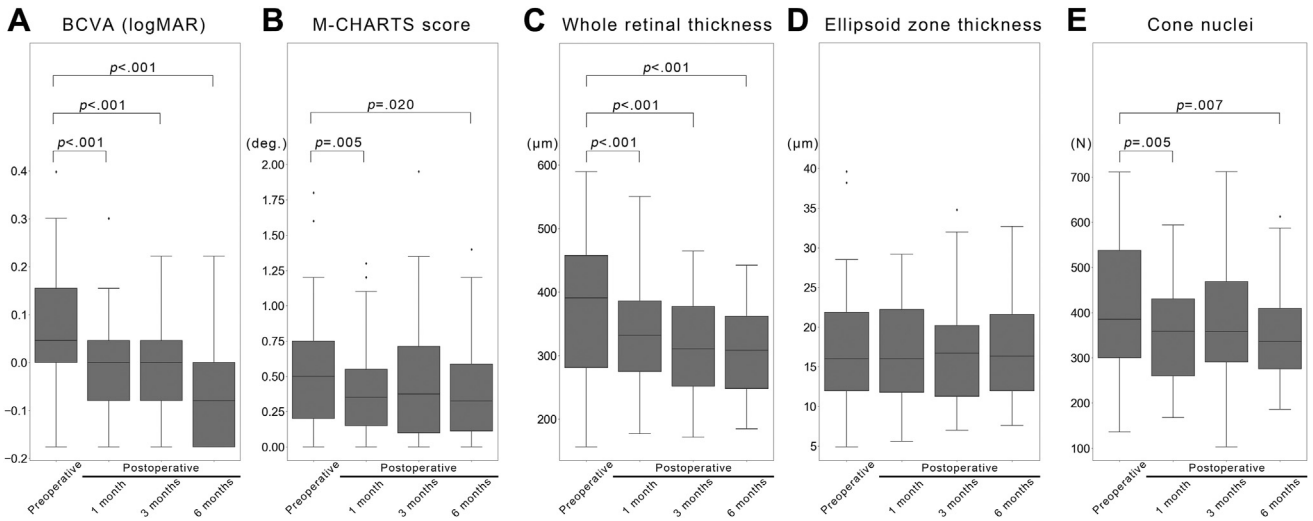

Figure 2. Longitudinal changes in visual function and foveal morphology at baseline and 1, 3, and 6 months postoperatively. This figure presents box-and-whisker plots comparing measurements at baseline and at 1, 3, and 6 months postoperatively. (**A**) Box-and-whisker plots of visual acuity measured by the logarithm of the minimal angle of resolution (logMAR). (**B**) Box-and-whisker plots of M-CHARTS scores. (**C**) Box-and-whisker plots of whole retinal thickness. (**D**) Box-and-whisker plots of ellipsoid zone band thickness. (**E**) Box-and-whisker plots of cone cell nuclei count. The statistical significance of the changes across the time points is highlighted in the figure. The *P* values are provided for comparative analysis between the preoperative measurements and those acquired at 1, 3, and 6 months postoperatively. Only findings with *P* values < 0.05 are marked to denote statistical significance. BCVA = best-corrected visual acuity.

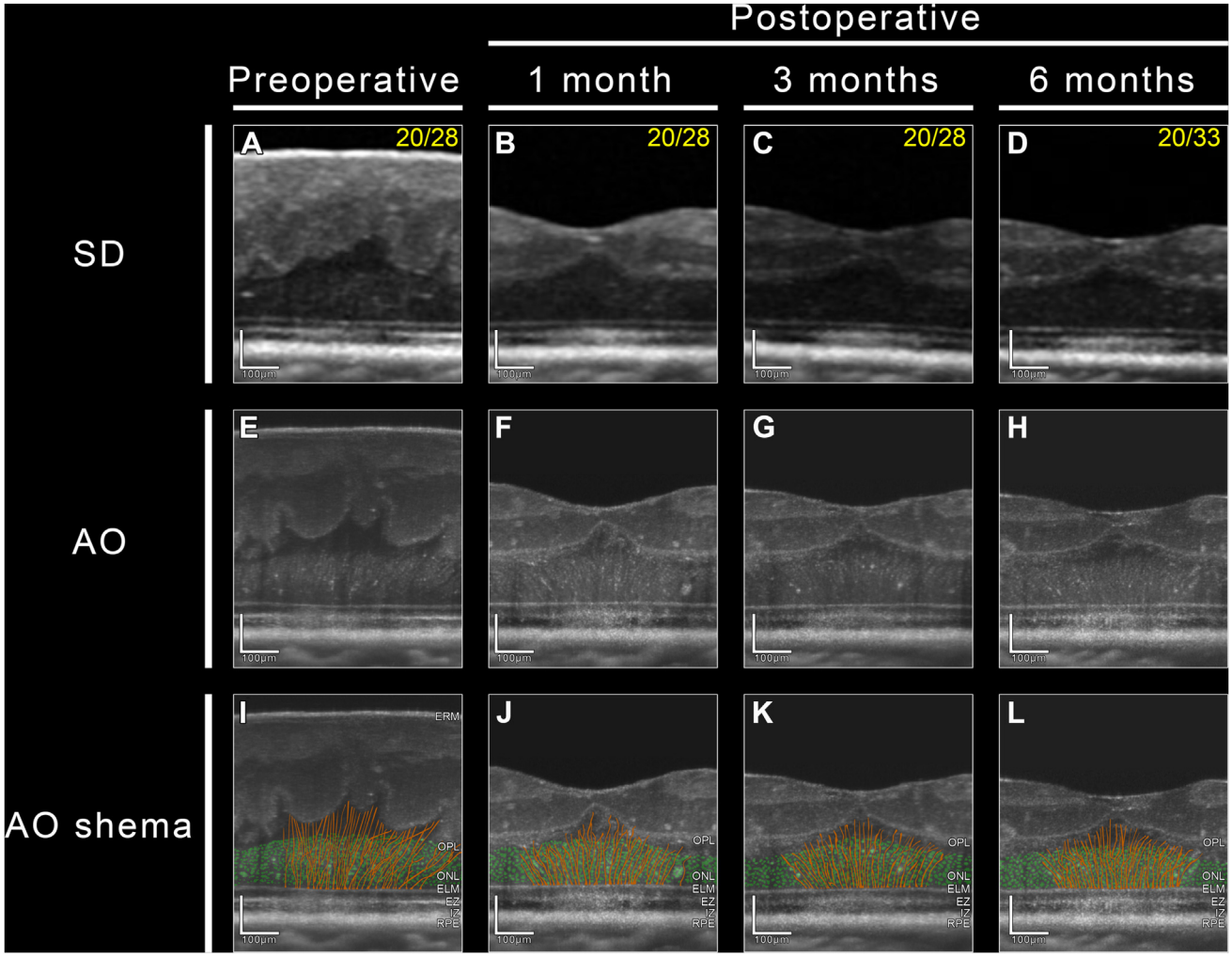

Figure 3. Foveal microstructural changes in an eye with epiretinal membrane from the preoperative period to 1, 3, and 6 months postoperatively. (**A**–**D**) Spectral-domain (SD) OCT images of an eye with epiretinal membrane (ERM) at the preoperative baseline and 1, 3, and 6 months postoperatively. (**E**–**H**) Adaptive optics (AO) OCT images of an eye with ERM at the preoperative baseline and 1, 3, and 6 months postoperatively. (**I**–**L**) Schemas generated from **E**–**H**, depicting cone cell nuclei as green areas and the visualized segment of Müller cells, from the outer plexiform layer (OPL) to the external limiting membrane (ELM), as orange areas. The preoperative and postoperative Snellen visual acuity at 1, 3, and 6 months postoperatively were 20/28, 20/28, 20/28, and 20/33, respectively. Notably, features such as cone cell nuclei, Müller cells and their pathways, vertical thickening of the ellipsoid zone (EZ) band (which emerged as a significant indicator of impaired visual acuity in this study), and outer segment discs were substantially clearer in AO-OCT images than in their SD-OCT counterparts throughout the observation period. IZ = interdigitation zone; ONL = outer nuclear layer; RPE = retinal pigment epithelium.

months postoperatively ($P = 0.007$, Fig 2), whereas the EZ thickness remained unchanged (Figs 2 and 4).

Associations between Preoperative and Postoperative Visual Functions and OCT Parameters

Tables 2 and 3 demonstrate the associations between visual function and OCT findings. The preoperative stage in the inner retina, specifically the change from stage 2 to stage 3, had a significantly worse preoperative BCVA ($P = 0.04$). Preoperatively, within the AO-OCT parameters, greater EZ thickness was associated with poorer BCVA ($P = 0.012$), whereas a higher cone nuclei count correlated with worse M-CHARTS scores ($P = 0.004$). The same trend was observed at 6 months postoperatively: greater EZ thickness was associated with poorer BCVA ($P = 0.014$), and a higher cone nuclei count correlated with worse M-CHARTS scores ($P = 0.010$).

Associations between the Preoperative OCT Metrics and Postoperative Visual Outcomes

Table 4 presents the correlation between the initial OCT findings and 6-month postoperative visual outcomes. Greater EZ thickness on preoperative AO-OCT was significantly associated with poorer postoperative BCVA ($P = 0.005$).

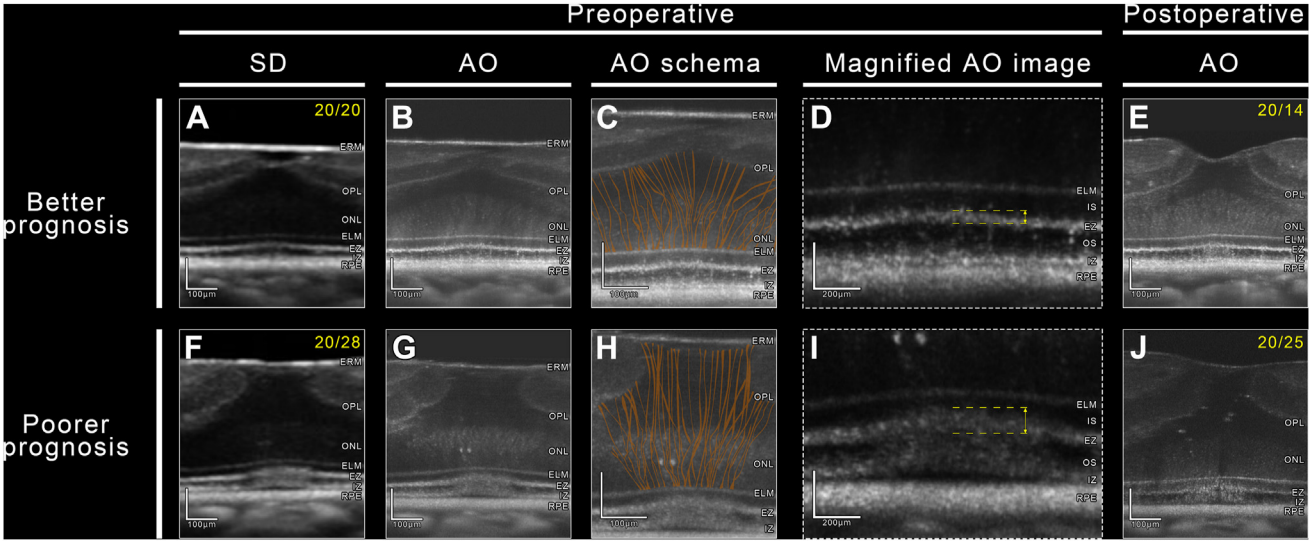

Figure 4. Visual prognosis variability in eyes with epiretinal membrane (ERM). Top: An eye with an ERM with a favorable visual prognosis. (**A**) A spectral-domain (SD) OCT image at the preoperative baseline. (**B**) An adaptive optics (AO) OCT image at the preoperative baseline. (**C**) A schema generated from **B**, depicting visualized segment of Müller cells, from the outer plexiform layer (OPL) to the external limiting membrane (ELM), as orange areas. (**D**) A magnified AO-OCT image of **B** at outer retinal layer. (**E**). An AO-OCT image at the 6 months postoperatively. The preoperative Snellen visual acuity is 20/20 with an unaltered photoreceptor layer and a distinct horizontally-oriented ellipsoid zone (EZ) band without vertical thickening (**D**). Visual acuity improved to 20/14 postoperatively, and the EZ band retained the sharp definition (**E**). Bottom: A case of ERM associated with a less favorable visual prognosis. (**F**) A SD-OCT image at the preoperative baseline. (**G**) An AO-OCT image at the preoperative baseline. (**H**) A schema generated from **G**, depicting visualized segment of Müller cells, from the OPL to the ELM, as orange areas. (**I**) A magnified AO-OCT image of **G** at the outer retinal layer. (**J**) An AO-OCT image at 6 months postoperatively. The preoperative Snellen visual acuity was 20/28, with the ERM causing vertical traction of the photoreceptor layer, as evidenced by a thickened, hyper-reflective EZ band (**I**). Visual acuity improved to 20/25 postoperatively; however, the thickening of the EZ band persisted (**J**). Both cases included SD-OCT and AO-OCT images, with a schematic representation of the AO-OCT findings and a detailed view of the EZ band is highlighted in yellow for enhanced visualization. IZ = interdigitation zone; ONL = outer nuclear layer; RPE = retinal pigment epithelium.

Discussion

In this study, we aimed to evaluate cellular alterations in the foveal neuroglia of eyes with idiopathic ERM, examine their correlation with visual function, and identify prognostic markers for visual outcomes postvitrectomy. Observations in eyes with ERM before surgery revealed notable differences in retinal structure when compared with healthy eyes. These differences included a highly reflective membrane at the vitreoretinal interface, predominantly vertical orientation of Müller cells, increased cone cell nuclei count, and EZ thickening. Following the uncomplicated surgical removal of both the ERM and ILM, postoperative imaging showed the resolution of the highly reflective areas at the vitreoretinal interface and a shift in Müller cells orientation toward a more diagonal, and seemingly normal, pattern. Interestingly, EZ thickness remained constant before and after the surgery. These observations demonstrated the potential evidence of the surgery's role in alleviating tractional forces associated with the presence of ERM. In addition, we observed that preoperative EZ thickness was associated with both preoperative and postoperative visual acuity. Similarly, postoperative EZ thickness showed an association with postoperative visual acuity. The number of cone nuclei observed preoperatively correlated with the degree of preoperative metamorphopsia, whereas the number observed postoperatively correlated with the degree of postoperative metamorphopsia.

The decrease in cone density postoperatively, alongside improved visual outcomes, may initially seem paradoxical. However, this can be understood within the context of ERM's impact on retinal structures. The initial increase in cone density likely reflects the effect of the centripetal force exerted by the ERM on the photoreceptor cells, causing a pathological elevation. The surgical ERM removal and subsequent relaxation of this force allow the retinal structure, including the photoreceptor layer, to normalize; hence, the previously elevated cone density decreases to physiological levels. We hypothesize that this normalization process, evident postoperatively, contributes to the observed improvements in visual function. Thus, the postoperative reduction in cone density signifies a restoration of a more normal retinal structure, which is associated with enhanced visual outcomes.

Recent developments in the field of ERM research can be attributed to SD-OCT findings,[19] which suggest a possible correlation between visual function and retinal structure and enhance our understanding of the pathogenesis of ERM. However, the reliable prediction of the postoperative visual outcomes in clinical settings hinges on the clarity of preoperative retinal changes. Marked alterations observed preoperatively indicate modest visual improvement. The progression of ERM varies, with many cases remaining stable or showing minimal symptoms. However, given the nonself-resolving nature of ERM,[20,21] early intervention may

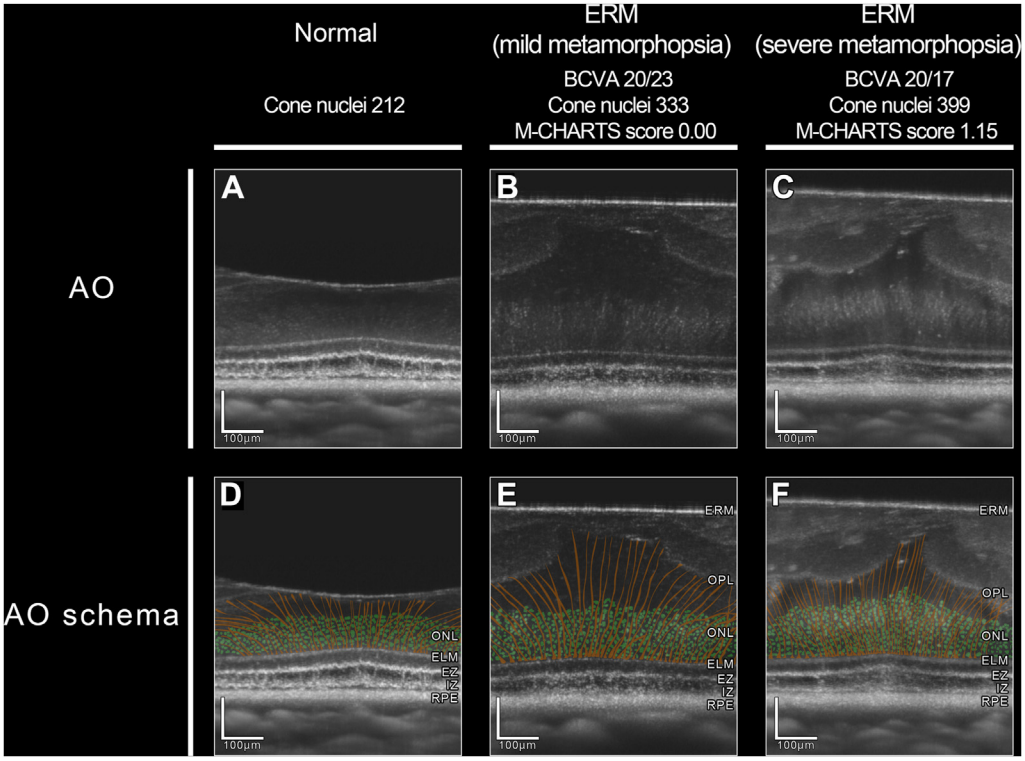

Figure 5. Adaptive optics OCT (AO-OCT) images illustrating associations between retinal neuroglial changes and M-CHARTS score. The AO-OCT images show a healthy eye (left) and eyes with an epiretinal membrane (ERM) manifesting mild metamorphopsia (middle) and severe metamorphopsia (right). **A**–**C**: AO-OCT images. **D**–**F**: A schema generated from **A**–**C**, depicting cone cell nuclei as green areas and the visualized segment of Müller cells, from the outer plexiform layer (OPL) to the external limiting membrane (ELM), as orange areas. The preoperative best-corrected visual acuity (BCVA) and M-CHARTS scores were 20/23 and 0.0, respectively, for the eye with mild metamorphopsia (middle) and 20/17 and 1.15, respectively, for the eye with severe metamorphopsia (right). The cone nuclei counts were 212, 333, and 399 in the healthy eye, the eye with mild metamorphopsia, and the eye with severe metamorphopsia, respectively. Notably, there was an increase in the cone nuclei count and vertical orientation of the Müller cells in the fovea in eyes with ERM compared with that in the healthy eyes. Moreover, the eyes with severe metamorphopsia had more cone nuclei than those with mild metamorphopsia. EZ = ellipsoid zone; IZ = interdigitation zone; ONL = outer nuclear layer; RPE = retinal pigment epithelium.

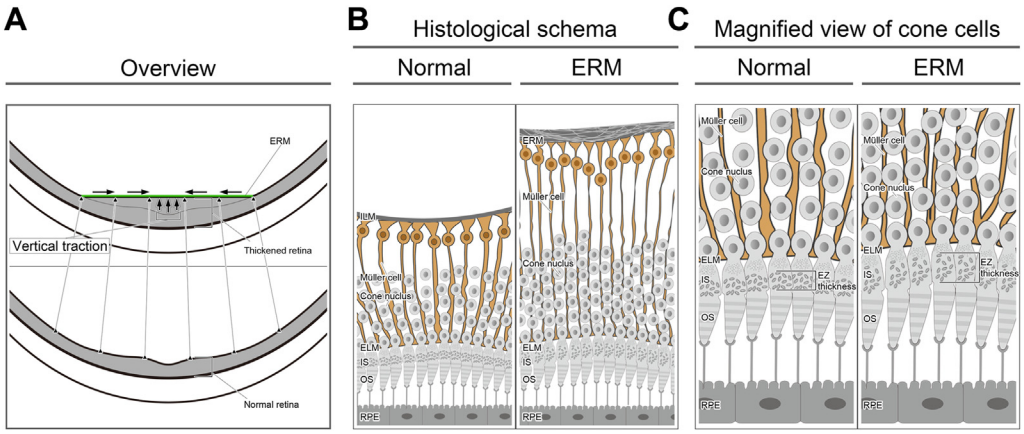

Figure 6. Schematic depictions of photoreceptor impairment due to epiretinal membrane (ERM). (**A**) A schematic overview of an eye affected by ERM. (**B**) Comparative histological schemas of a healthy eye versus an eye with ERM. (**C**) Detailed schematic representations of the cone cells in a healthy eye and an eye with ERM. In the ERM-affected eye, vertical traction is depicted, originating from a horizontal contractive force on the retinal surface. This force is vertically and anteriorly oriented, influenced by posteriorly convex shape of the fovea. Through the inner limiting membrane (ILM; basal membrane of Müller cells), ERM exerts anterior and vertical traction on Müller cells, which is then transferred to the adjacent photoreceptors. When traction is pronounced, the integrity of the ellipsoid zone (EZ) band is affected, which can lead to decreased visual acuity. ELM = external limiting membrane; RPE = retinal pigment epithelium.

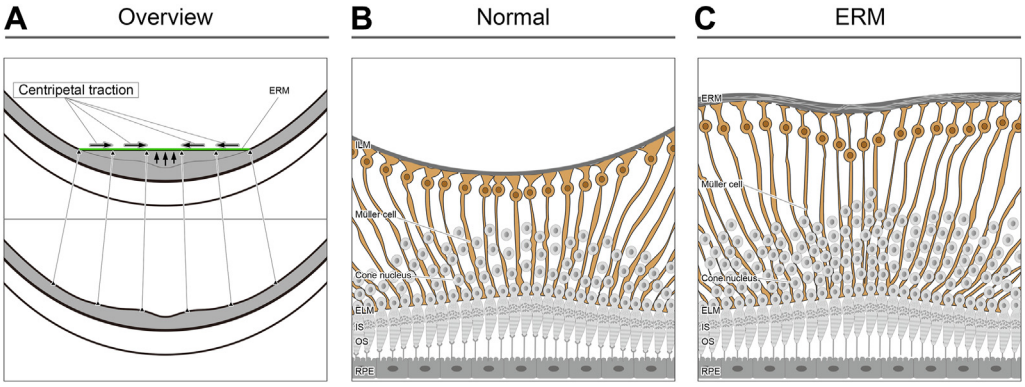

Figure 7. Schematic illustrations of metamorphopsia due to epiretinal membrane (ERM). (**A**) Schematic representation of an eye with an ERM. (**B**) Diagram of a healthy retinal structure. (**C**) An eye with ERM exhibiting features of metamorphopsia. Horizontal contractive forces applied by the ERM distort the retinal neuroglia. This distortion is evidenced by the altered orientation of Müller cells, which extend from the retinal surface to the deeper layers, and by the increased density of cone nuclei within the outer nuclear layer. While these changes were not directly correlated with visual acuity, they were significantly associated with the severity of metamorphopsia, as quantified by the M-CHARTS score. ELM = external limiting membrane; ILM = inner limiting membrane; RPE = retinal pigment epithelium.

benefit patients in whom the disease progression significantly affects visual function. Although precise evaluation of retinal structure using OCT does not directly reveal changes in visual function, integrating these structural assessment results with those from visual function tests, such as VA and M-charts, facilitates a more comprehensive understanding of the relationship between structural alterations and functional abnormalities.

Conversely, the EZ thickness did not show a significant association with the M-CHARTS score preoperatively and postoperatively. In addition, the density of cone cell nuclei showed no significant correlation with the BCVA at either time point. These differential associations between the AO-OCT parameters and types of visual impairment indicate that reduced visual acuity and metamorphopsia may result from distinct morphological alterations. Epiretinal membrane-induced contractile forces at the vitreoretinal interface have a significant effect on retinal neuroglia.[22,23] The influence of these forces might be further modified by the natural shape of the eye and the arrangement of neural support cells within the retina.[11,24] Müller cells are structural elements within the retina[25,26] that potentially regulate the photoreceptor activity that is vital for visual acuity,[27–29] which ERM may compromise. Moreover, studies using SD-OCT have underscored the significance of the foveal EZ in appraising visual acuity in eyes with ERM.[10,11,19,30] The appearance of the central bouquet abnormality[11] in the photoreceptor layer is suggestive of the presence of vertical traction exerted by the Müller cells. Our findings, which show the association between increased EZ thickness and visual acuity, provide a direct view of this tractional effect.

Examination of ERM-induced contractile forces, acting in conjunction with the retinal plane, may include the assessment of the depth of the inner retinal folds[31,32] and the

Table 2. Associations between Preoperative Visual Functions and OCT Findings

	Preoperative Visual Functions			
	BCVA (logMAR)		M CHARTS Score (degree)	
	Standardized β ($\times 10^{-2}$)		Standardized β ($\times 10^{-2}$)	
Preoperative OCT	(95% CI)	P Value	(95% CI)	P Value
Spectral domain				
Inner retina				
Stage 2 to stage 1	19.2 (−14.0 to 52.3)	0.25	−29.9 (−66.2 to 6.3)	0.10
Stage 3 to stage 2	31.0 (1.4–60.5)	0.04	26.8 (−5.9 to 59.5)	0.11
Outer retina				
Presence of cotton ball sign	−8.7 (−41.8 to 24.4)	0.60	27.3 (−9.0 to 63.5)	0.14
Presence of foveolar detachment	7.3 (−23.3 to 38.0)	0.63	−14.1 (−47.6 to 19.4)	0.40
Adaptive optics				
EZ thickness (μm)	36.2 (8.6–63.9)	0.012	−13.6 (−44.0 to 16.8)	0.38
Cone cell nuclei (n)	0.6 (−28.4 to 29.5)	0.97	48.8 (16.9–80.6)	0.004

BCVA = best corrected visual acuity; CI = confidence interval; EZ = ellipsoid zone; logMAR = logarithm of minimum angle of resolution.

Table 3. Associations between the 6-Month Postoperative Visual Function and OCT Findings

	Postoperative Visual Functions			
	BCVA (logMAR)		*M CHARTS Score (Degree)*	
	Standardized β ($\times 10^{-2}$)		*Standardized β ($\times 10^{-2}$)*	
Postoperative OCT	*(95% CI)*	P *Value*	*(95% CI)*	P *Value*
Spectral domain				
Whole retinal thickness	−11.7 (−42.5 to 19.1)	0.45	−8.4 (−38.6 to 21.8)	0.58
Presence of cotton ball sign	10.1 (−19.6 to 39.7)	0.50	5.4 (−23.7 to 34.5)	0.71
Adaptive optics				
EZ thickness (μm)	42.1 (9.0–75.2)	0.014	13.1 (−19.4 to 45.5)	0.42
Cone cell nuclei (n)	−2.9 (−33.1 to 27.4)	0.85	39.7 (10.0–69.4)	0.010

BCVA = best corrected visual acuity; CI = confidence interval; EZ = ellipsoid zone; logMAR = logarithm of minimum angle of resolution.

degree of foveal vascular zone reduction.[33–35] Ooto et al reported the relationship between structural changes within the photoreceptor mosaic and visual function, particularly highlighting the link between metamorphopsia and such structural alterations.[36] Our study demonstrated an association between the density of cone cell nuclei and severity of metamorphopsia, which builds upon and extends the insights gained from earlier research utilizing SD-OCT and AO-scanning laser ophthalmoscopy.

This study had certain limitations that must be acknowledged when interpreting the findings. First, this was a longitudinal study; however, the observation period was confined to merely 6 months. Consequently, although a clear trend of recovery in visual function was observed during this period, the longer-term prognosis remains unknown. Furthermore, AO-OCT offers a relatively limited field of view; thus, the correlations outlined in this study may not have captured all visual functions. The changes in cone photoreceptors, especially the nuclear density and findings associated with EZ, as well as the length and course of the Müller cells, were the focus of our study. The assessment of Müller cell orientation required a degree of subjective interpretation due to the lack of a quantifiable measurement approach. This reliance on subjective analysis could potentially influence the results of the study by introducing a degree of interpretation bias. These parameters showed significant associations with visual acuity and metamorphopsia. However, our analysis did not include other retinal neuroglial cells, such as bipolar, ganglion, amacrine, and horizontal cells, which may have introduced potential gaps in our understanding. Although visual impairments associated with ERM are not restricted to decreased visual acuity and metamorphopsia, the present study did not include symptoms such as macropsia and micropsia. Finally, the widespread applicability of SD-OCT, which is suitable for various contexts, contrasts significantly with the specialized nature of AO-OCT. This difference in usability emphasizes that the findings of the present study must be extrapolated with caution.

In conclusion, our study demonstrated that the contractile forces of ERM apply multidimensional traction to the retinal

Table 4. Association between the 6-Month Postoperative Visual Outcomes and Preoperative OCT Findings

	Postoperative Visual Functions (Month 6)			
	BCVA (logMAR)		*M CHARTS Score (Degree)*	
	Standardized β ($\times 10^{-2}$)		*Standardized β ($\times 10^{-2}$)*	
Preoperative OCT	*(95% CI)*	P *Value*	*(95% CI)*	P *Value*
Spectral domain				
Inner retina				
Stage 2 to stage 1	8.4 (−29.0 to 45.8)	0.65	−0.3 (−39.0 to 38.3)	0.99
Stage 3 to stage 2	1.9 (−31.5 to 35.2)	0.91	18.4 (−16.1 to 52.8)	0.29
Outer retina				
Presence of cotton ball sign	7.0 (−30.4 to 44.4)	0.71	26.1 (−12.5 to 64.7)	0.18
Presence of foveolar detachment	−12.4 (−47.0 to 22.1)	0.47	−14.9 (−50.6 to 20.8)	0.40
Adaptive optics				
EZ thickness (μm)	45.5 (14.2–76.7)	0.005	18.2 (−14.1 to 50.5)	0.26
Cone cell nuclei (n)	−10.5 (−43.2 to 22.1)	0.52	5.9 (−27.9 to 39.7)	0.73

BCVA = best corrected visual acuity; CI = confidence interval; EZ = ellipsoid zone; logMAR = logarithm of minimum angle of resolution.

tissue. These forces, which comprise transverse and axial components, result in observable changes in the orientation and morphology of the Müller cells, changes in the cone nuclei density, and alterations in the foveal EZ thickness. Moreover, these structural alterations correspond to the changes in visual acuity and the severity of metamorphopsia, as documented in patients preoperatively and postoperatively.

Footnotes and Disclosures

Originally received: January 23, 2024.
Final revision: April 10, 2024.
Accepted: April 15, 2024.
Available online: April 22, 2024. Manuscript no. XOPS-D-24-00028.

Department of Ophthalmology and Visual Sciences, Kyoto University Graduate School of Medicine, Kyoto, Japan.

Disclosure(s):

All authors have completed and submitted the ICMJE disclosures form.

The authors made the following disclosures:

A.T.: Honoraria —Canon, Findex, Santen Pharmaceutical, Kowa Pharmaceutical, Pfizer, AMO Japan, Wakamoto Pharmaceutical, Alcon Japan, Otsuka Pharmaceutical, Nitten Pharmaceutical, Alcon Pharma, AbbVie GK, Senju Pharmaceutical, Bayer Yakuhin, Novartis Pharma.

M.H.: Honoraria — Novartis Pharma, Senju Pharmaceutical, Kyoto Drug Discovery & Development.

S.N.: Honoraria — Senju Pharmaceutical, Kowa Pharmaceutical, Santen Pharmaceutical.

S.O.: Honoraria — Bayer Yakuhin, Kowa Pharmaceutical, Janssen Pharmaceutical, Novartis Pharma, AMO Japan, Santen Pharmaceutical, Alcon Japan, Senju Pharmaceutical.

Y.M.: Honoraria — Rohto Pharmaceutical, Bayer Yakuhin, Novartis Pharma, Alcon Japan, Canon, Santen Pharmaceutical, Senju Pharmaceutical, AMO Japan, HOYA, Johnson & Johnson K.K.

This study was supported in part by Canon Inc. (Tokyo, Japan). The funders had no role in the study design, data collection and analysis, decision to publish, or preparation of the manuscript.

HUMAN SUBJECTS: Human subjects were included in this study. This prospective, longitudinal study was conducted in strict accordance with the tenets of the Declaration of Helsinki. This study was approved by the Institutional Review Board and Ethics Committee of the Kyoto University Graduate School of Medicine (Kyoto, Japan). Written informed consent was obtained from the patients and healthy volunteers before commencing any study-related procedure or evaluation.

No animal subjects were used in this study.

Author Contributions:

Conception and design: Ishikura, Muraoka, Hata, Ishihara, Ooto, Tsujikawa

Data collection: Ishikura, Nishigori, Kogo, Akiyama, Numa

Analysis and interpretation: Ishikura, Nishigori, Kogo, Akiyama, Numa, Hata, Ishihara, Ooto, Tsujikawa

Obtained funding: N/A

Overall responsibility: Ishikura, Muraoka

Abbreviations and Acronyms:
AO = adaptive optics; **BCVA** = best-corrected visual acuity; **ERM** = epiretinal membrane; **EZ** = ellipsoid zone; **ILM** = inner limiting membrane; **SD** = spectral-domain.

Keywords:
Adaptive optics, Adaptive optics optical coherence tomography, Ellipsoid zone, Epiretinal membrane, Müller cell.

Correspondence:
Yuki Muraoka, MD, PhD, Department of Ophthalmology, Kyoto University Graduate School of Medicine, Sakyo-ku, Kyoto 606-8507, Japan. E-mail: muraoka@kuhp.kyoto-u.ac.jp.

References

1. Ng CH, Cheung N, Wang JJ, et al. Prevalence and risk factors for epiretinal membranes in a multi-ethnic United States population. *Ophthalmology*. 2011;118:694–699.
2. Miyazaki M, Nakamura H, Kubo M, et al. Prevalence and risk factors for epiretinal membranes in a Japanese population: the Hisayama study. *Graefes Arch Clin Exp Ophthalmol*. 2003;241:642–646.
3. Hiscott P, Hagan S, Heathcote L, et al. Pathobiology of epiretinal and subretinal membranes: possible roles for the matricellular proteins thrombospondin 1 and osteonectin (SPARC). *Eye (Lond)*. 2002;16:393–403.
4. Snead DR, James S, Snead MP. Pathological changes in the vitreoretinal junction 1: epiretinal membrane formation. *Eye (Lond)*. 2008;22:1310–1317.
5. Weinberger D, Stiebel-Kalish H, Priel E, et al. Digital red-free photography for the evaluation of retinal blood vessel displacement in epiretinal membrane. *Ophthalmology*. 1999;106:1380–1383.
6. Koizumi H, Spaide RF, Fisher YL, et al. Three-dimensional evaluation of vitreomacular traction and epiretinal membrane using spectral-domain optical coherence tomography. *Am J Ophthalmol*. 2008;145:509–517.
7. Sakai D, Takagi S, Hirami Y, et al. Correlation between tangential distortion of the outer retinal layer and metamorphopsia in patients with epiretinal membrane. *Graefes Arch Clin Exp Ophthalmol*. 2021;259:1751–1758.
8. Mavi Yildiz A, Avci R, Yilmaz S. The predictive value of ectopic inner retinal layer staging scheme for idiopathic epiretinal membrane: surgical results at 12 months. *Eye (Lond)*. 2021;35:2164–2172.
9. Govetto A, Lalane 3rd RA, Sarraf D, et al. Insights into epiretinal membranes: presence of ectopic inner foveal layers and a new optical coherence tomography staging scheme. *Am J Ophthalmol*. 2017;175:99–113.
10. Tsunoda K, Watanabe K, Akiyama K, et al. Highly reflective foveal region in optical coherence tomography in eyes with vitreomacular traction or epiretinal membrane. *Ophthalmology*. 2012;119:581–587.
11. Govetto A, Bhavsar KV, Virgili G, et al. Tractional abnormalities of the central foveal bouquet in epiretinal membranes: clinical spectrum and pathophysiological perspectives. *Am J Ophthalmol*. 2017;184:167–180.
12. Roorda A, Williams DR. The arrangement of the three cone classes in the living human eye. *Nature*. 1999;397:520–592.
13. Kadomoto S, Uji A, Arichika S, et al. Macular cone abnormalities in Behçet's disease detected by adaptive optics scanning light ophthalmoscope. *Ophthalmic Surg Lasers Imaging Retina*. 2021;52:218–225.

14. Ishikura M, Muraoka Y, Kadomoto S, et al. Retinal arterial macroaneurysm rupture caused by dissection-like change in the vessel wall. *Am J Ophthalmol Case Rep*. 2022;25:101346.
15. Kadomoto S, Muraoka Y, Uji A, et al. Human foveal cone and Mülller cells examined by adaptive optics optical coherence tomography. *Transl Vis Sci Technol*. 2021;10:17.
16. Ishikura M, Muraoka Y, Kadomoto S, et al. Evaluation of foveal cone and Müller cells in epiretinal membrane using adaptive optics OCT. *Ophthalmol Sci*. 2023;4:100362.
17. Ishikura M, Muraoka Y, Nishigori N, et al. Widefield choroidal thickness of eyes with central serous chorioretinopathy examined by swept-source OCT. *Ophthalmol Retina*. 2022;6:949−956.
18. Bennett AG, Rudnicka AR, Edgar DF. Improvements on Littmann's method of determining the size of retinal features by fundus photography. *Graefes Arch Clin Exp Ophthalmol*. 1994;232:361−367.
19. Shimozono M, Oishi A, Hata M, et al. The significance of cone outer segment tips as a prognostic factor in epiretinal membrane surgery. *Am J Ophthalmol*. 2012;153:698−704, 704.e1.
20. Byon IS, Pak GY, Kwon HJ, et al. Natural history of idiopathic epiretinal membrane in eyes with good vision assessed by spectral-domain optical coherence tomography. *Ophthalmologica*. 2015;234:91−100.
21. Nishi Y, Shinoda H, Uchida A, et al. Detection of early visual impairment in patients with epiretinal membrane. *Acta Ophthalmol*. 2013;91:e353−e357.
22. Heilskov TW, Massicotte SJ, Folk JC. Epiretinal macular membranes in eyes with attached posterior cortical vitreous. *Retina*. 1996;16:279−284.
23. Gandorfer A, Rohleder M, Kampik A. Epiretinal pathology of vitreomacular traction syndrome. *Br J Ophthalmol*. 2002;86:902−909.
24. Kim JH, Kim YM, Chung EJ, et al. Structural and functional predictors of visual outcome of epiretinal membrane surgery. *Am J Ophthalmol*. 2012;153:103−110.e1.
25. Syrbe S, Kuhrt H, Gärtner U, et al. Müller glial cells of the primate foveola: an electron microscopical study. *Exp Eye Res*. 2018;167:110−117.
26. Gass JD. Müller cell cone, an overlooked part of the anatomy of the fovea centralis: hypotheses concerning its role in the pathogenesis of macular hole and foveomacualr retinoschisis. *Arch Ophthalmol*. 1999;117:821−823.
27. Franze K, Grosche J, Skatchkov SN, et al. Muller cells are living optical fibers in the vertebrate retina. *Proc Natl Acad Sci USA*. 2007;104:8287−8292.
28. Pow DV, Crook DK. Direct immunocytochemical evidence for the transfer of glutamine from glial cells to neurons: use of specific antibodies directed against the d-stereoisomers of glutamate and glutamine. *Neuroscience*. 1996;70:295−302.
29. Rich KA, Figueroa SL, Zhan Y, Blanks JC. Effects of Müller cell disruption on mouse photoreceptor cell development. *Exp Eye Res*. 1995;61:235−248.
30. Fang IM, Hsu CC, Chen LL. Correlation between visual acuity changes and optical coherence tomography morphological findings in idiopathic epiretinal membranes. *Graefes Arch Clin Exp Ophthalmol*. 2016;254:437−444.
31. Kanzaki Y, Matoba R, Kimura S, et al. Epiretinal membrane impairs the inner retinal layer in a traction force-dependent manner. *Ophthalmol Sci*. 2023;3:100312.
32. Okamoto F, Sugiura Y, Okamoto Y, et al. Associations between metamorphopsia and foveal microstructure in patients with epiretinal membrane. *Invest Ophthalmol Vis Sci*. 2012;53:6770−6775.
33. Kumagai K, Furukawa M, Suetsugu T, Ogino N. Foveal avascular zone area after internal limiting membrane peeling for epiretinal membrane and macular hole compared with that of fellow eyes and healthy controls. *Retina*. 2018;38:1786−1794.
34. Okamoto F, Sugiura Y, Okamoto Y, et al. Time course of changes in aniseikonia and foveal microstructure after vitrectomy for epiretinal membrane. *Ophthalmology*. 2014;121:2255−2260.
35. Hirata A, Nakada H, Mine K, et al. Relationship between the morphology of the foveal avascular zone and the degree of aniseikonia before and after vitrectomy in patients with unilateral epiretinal membrane. *Graefes Arch Clin Exp Ophthalmol*. 2019;257:507−515.
36. Ooto S, Hangai M, Takayama K, et al. High-resolution imaging of the photoreceptor layer in epiretinal membrane using adaptive optics scanning laser ophthalmoscopy. *Ophthalmology*. 2011;118:873−881.